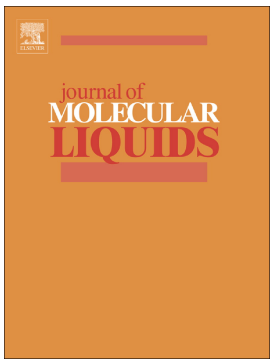

Design and synthesis of novel ribofuranose nucleoside analogues as antiproliferative agents: A molecular docking and DFT study

Çiğdem Karabacak Atay, Tahir Tilki, Bülent Dede

PII: S0167-7322(18)32548-0
DOI: doi:10.1016/j.molliq.2018.08.009
Reference: MOLLIQ 9454

To appear in: *Journal of Molecular Liquids*

Received date: 17 May 2018
Revised date: 31 July 2018
Accepted date: 1 August 2018

Please cite this article as: Çiğdem Karabacak Atay, Tahir Tilki, Bülent Dede , Design and synthesis of novel ribofuranose nucleoside analogues as antiproliferative agents: A molecular docking and DFT study. Molliq (2018), doi:10.1016/j.molliq.2018.08.009

DESIGN AND SYNTHESIS OF NOVEL RIBOFURANOSE NUCLEOSIDE ANALOGUES AS ANTIPROLIFERATIVE AGENTS: A MOLECULAR DOCKING AND DFT STUDY

Çiğdem KARABACAK ATAY[1], Tahir TİLKİ[2], Bülent DEDE[2*]

[1]*Mehmet Akif Ersoy University, Faculty of Education, Department, of Basic Education, 15030, Burdur, Turkey*

[2]*Süleyman Demirel University, Faculty of Science & Art, Department of Chemistry, 32260, Isparta, Turkey*

*bulentdede@sdu.edu.tr

Corresponding author

Telephone : +90 246 2114153

Fax : +90 246 2114399

Abstract

The new analogues of ribofuranose fused heterocyclic compounds were synthesized a series of diazotization, cyclization, coupling and hydrolysis reactions and structures were characterized by spectroscopic methods. To explain the spectroscopic properties in detail, such as molecular geometric parameters, vibrational wavenumbers, HOMO-LUMO energies, ^{1}H-NMR chemical shift values and electronic transitions, density functional theory (DFT) calculations were used. The structural and spectroscopic data of the molecules in the ground state were calculated by DFT using B3LYP functional with 6-311G(d,p) basis set. Isotropic chemical shifts were calculated using the gauge-invariant atomic orbital (GIAO) method. Furthermore molecular docking (ligand–protein) simulations were performed to obtain antiproliferative activity of the synthesized ribofuranose nucleoside analogues against epidermal growth factor receptor and vascular endothelial growth factor receptor 2. Full fitness score and binding energy length values revealed that studied three compounds can act as potential inhibitor against selected receptors.

Keywords: Nucleoside, DFT, molecular docking, antiproliferative, anticancer

1. Introduction

Cancer is the most important health problem in the 21st century. The incidence of cancer in many countries has even caught heart disease. Cancer is the name of the illness that is caused by the deterioration of some organs or tissue cells in one day by going out of control and tending to irregularity in a harmonious state of our body which is governed by strict control mechanisms. Today, cancer has become a common disease that can be caught for the life of one of every three people today. The number of cancer-affected patients is increasing all over the world. Therefore, the studies on the synthesis of new and effective anticancer agents are very important and increasing. Modified nucleosides have attracted interest in recent years because the showing interesting biological properties such as antiviral and anticancer agents. Nucleoside analogues are among the first chemotherapeutic agents used in cancer treatment. Finding new drugs is a very expensive and time-consuming process. Although there are too many candidate molecules with potency to be drug, the experiments that have to be performed for each cause the drug cost to increase and the prolongation of the duration of the drug to be taken [1-4].

At this point, the molecular docking method is at the forefront. In structure-based drug design, molecular docking is the most common and has been widely used since the early 1980s [5]. The molecular docking approach can be used to model the interaction between a small molecule and a protein at the atomic level, which allow us to characterize the behaviour of small molecules in the binding site of target proteins as well as to elucidate fundamental biochemical processes [6].

The protein bound by the epidermal growth factor on the surface of some cells causes the cells to divide. Since the epidermal growth factor is present at high levels abnormally on many cancer cell surfaces, these cells may be severely disrupted in the presence of epidermal growth factor. Activation of receptors by growth factors in the proliferation of tumour cells is an important step. Epidermal growth factor receptor (EGFR) inhibitors are highly effective agents in the treatment of metastatic epithelial cancers [7,8].

The vascular endothelial growth factor (VEGF) family of peptide growth factors and receptors are key regulators of tumour growth and metastatic dissemination [9]. Vascular endothelial growth factor receptor 2 (VEGFR2) is a type V receptor tyrosine kinase mainly known to be expressed in vascular endothelial cells and encoded by the KDR (kinase insert domain receptor) gene [10]. VEGFR2 is expressed in many but not all vascular endothelial cells from early fetal development, and it is more highly expressed in neovascular tumour endothelia than in normal endothelia [11,12]. Recently, the emergence of tyrosine kinase inhibitors with VEGFR2 specificity, such as sunitinib, sorafenib and cabozantinib, and VEGFR2 blocked with bevacizumab (analogous to herceptin in breast cancer) with a VEGF neutralizing antibody, suggests that these inhibitors may be effective against VEGFR2 [13-16]. Eventually blocking VEGFR2 signalling pathway has become an attractive approach for the treatment of cancers [17,18].

Based on the above consideration we synthesized novel analogues including both the ribofuranose and the heterocyclic base starting from nitro aniline derivatives to clarify the importance of sugar moiety. Quantum chemical calculations were carried out using the density functional theory (DFT) and experimental results were compared with the theoretical ones. To understand the interactions of synthesized nucleoside analogues at active sites of

epidermal growth factor receptor (PDB ID: 1M17) and vascular endothelial growth factor receptor 2 (PDB ID: 2XIR), molecular docking studies were also performed and reported in this paper.

2. Experimental

2.1. Experimental equipment

- Chemicals: purchased from Merck and Aldrich Chemical Company and used without further purification.
- FT-IR analysis: Shimadzu IR Prestige-21 Fourier Transforminfrared (FT-IR) spectrophotometer (on a KBr disk)
- Nuclear magnetic resonance (^{1}H-NMR) analysis: Bruker Ultrashield Superconducting 400 MHz
- Ultraviolet–visible (UV–vis) absorption analysis: Shimadzu UV-1601 double beam spectrophotometer
- Melting points: Electrothermal 9100 melting point apparatus

2.2. Synthesis of nucleosides 5a-c

o-, *m*-, *p*-nitro substitute aniline compounds **1a-c** (0.01 mol) was dissolved in hydrochloric acid and the solution was cooled to 0–5 ^{o}C. Then, sodium nitrite (0.01 mol) in water (20 mL) was added to this solution at 0–5 ^{o}C. The resulting diazonium solution was added to a stirred solution of ethylacetoacetate little by little; therewithal solid sodium acetate was added to maintain the pH at 7-8. This mixture was stirred at 0-5 ^{o}C for 4 h. The resulting solid **2a-c** was filtered, washed with cold water three times and dried. 0.005 mol solid **2a-c** and hydrazine hydrate were heated under reflux in ethanol for 8 h and the reaction mixture was saturated with water. The resulting solid product **3a-c** was filtrated and crystallized from DMF-H_2O.

Compounds **3a-c** were heated under reflux for 12 h in hexamethyldisilazane with $(NH_4)_2SO_4$. The solution was concentrated and in anhydrous 1,2-dichloroethane, residue was dissolved. Trimethylsilyl trifluoromethanesulfonate and 1-O-acetyl-2,3,5-tri-O-benzoyl-ß-D-ribofuranose were added to this solution. This mixture was stirred for 24 h at room temperature, washed three times, dried with sodium sulfate, filtered and evaporated. Recrystallization from DMF-H_2O gave crystals of dye 4a-c. Obtained compounds **4a-c** were dissolved in methanol–ammonia solution and for a week stirred at room temperature. Finally, to get the nucleosides **5a-c**, the mixture was evaporated and purified by crystallization from DMF-H_2O. (***5a***: Red solid, yield 76%, m.p. 96-98^oC, ***5b***: Yellow solid, yield 73%, m.p. 85-87^oC, ***5c***: Orange solid, yield 67%, m.p. 87-89^oC). The general route for the synthesis of nucleosides is shown in **Figure 1**.

2.3. Computational details

Calculations were carried out using Gaussian 09 and visualizations were performed by GaussView 5.0.9 program packages [19,20]. The molecular structure of the synthesized compounds in the ground state were optimized by the DFT method using B3LYP functional with 6-311G(d,p) basis set [21,22]. The simulated UV-vis spectra were performed at the time dependent density functional theory (TD-DFT) using B3LYP level with same basis set [23,24]. Contribution percentages of the excitations were calculated using GaussSum 3.0 program [25]. ^{1}H-NMR shielding constants were calculated by applying gauge-invariant atomic orbital (GIAO) method [26,27].

2.4. Molecular Docking Studies

The interactions of synthesized molecules with epidermal growth factor receptor (PDB ID: 1M17) and vascular endothelial growth factor receptor 2 (PDB ID: 2XIR) were analysed

using docking simulation. Modelling was performed on SwissDock web server using EADock DSS algorithm [28]. In the molecular docking studies, the optimized geometries from the theoretical calculations of the ligands were used. High resolution crystal structures of EGFR (PDB ID: 1M17) and VEGFR2 (PDB ID: 2XIR) were obtained from protein data bank (https://www.rcsb.org). All images in molecular docking studies were drawn with the UCSF Chimera package [29].

3. Results and Discussion

3.1. Spectral characteristics

Tautomerism is called the balance of compounds that can be converted into one to another. The most well-known tautomerism is the keto-enol tautomerism. The two forms can be transformed into one another by the action of alpha hydrogen and the displacement of the bonding electrons. Tautomeric forms of synthesized nucleosides **5a-c** were presented in **Figure 2.**

The FTIR spectra of nucleosides **5a-c** showed aliphatic (Alip.-H) band at 2960-2920 cm^{-1}, aromatic (Ar-H) band at 3190-3160 cm^{-1}, azo (N=N) band at 1570-1490 cm^{-1}, asymmetric N-O band at 1620-1610 cm^{-1}, symmetric N-O band at 1450 cm^{-1} and C-O band at 1250-1220 cm^{-1}. As corresponding B3LYP/6-311G(d,p) calculations, aliphatic (Alip.-H) band at 2919-2918 cm^{-1}, aromatic (Ar-H) band at 3122-3095 cm^{-1}, azo (N=N) band at 1546–1471 cm^{-1}, asymmetric N-O band at 1586-1585 cm^{-1}, symmetric N-O band at 1417-1416 cm^{-1} and C-O band at 1211-1123 cm^{-1} were recorded. Experimentally and theoretically FT-IR spectra of nucleoside **5a** was shown in **Figure 3** and nucleosides **5b-c** were given in **Figure S1**

(Supplementary data, Appendix A). Vibrational frequency values of nucleosides **5a-c** were given in **Table 1**, along with experimental and theoretical data. Small deviations were observed owing to the vibration bands complexity when the results were compared.

The linear regressions between the experimental and theoretical frequencies of nucleosides **(5a-c)** were displayed in **Figure 4**. The obtained equality by using the method of DFT/B3LYP for **5a-c** were y= 0.9858x (R^2=0.998), y= 0.9772x (R^2=0.9976), y= 0.98x (R^2=0.9998), respectively. These results showed us that the experimentally obtained frequency values were in agreement with the theoretically calculated frequency values.

^{1}H-NMR spectra of nucleosides **5a-c** showed broad peaks at 11.63-11.52 ppm (OH) of pyrazole and 4.71-3.79 ppm (OH) of ribofuranose, respectively. The other δ values of 2.50-2.08 ppm (pyrazole, CH_3), 5.29-5.08 ppm (ribofuranose, -CH), 5.53-5.51 ppm (ribofuranose, -CH_2) and 8.50-7.35 ppm (aromatic H) were recorded. ^{1}H-NMR spectra of nucleoside **5a** was given in **Figure 5** and nucleosides **5b-c** were illustrated in **Figure S2 (Supplementary data, Appendix A)**. Calculated by B3LYP/6-311G(d,p), chemical shift δ values of 2.37-2.33 ppm (pyrazole, CH_3), 5.69-4.02 ppm (ribofuranose, -CH), 4.12–4.11 ppm (ribofuranose, -CH_2) and 8.97-7.68 ppm (aromatic H) were obtained. Nucleosides **5a-c** showed peaks at 5.59-5.44 ppm (OH) of pyrazole and 1.67-0.63 ppm (OH) of ribofuranose. It is observed that the theoretical and experimental ^{1}H-NMR values are in harmony with each other except for –OH protons. This can be explained as follows: due to the tautomerization of the synthesized nucleosides, the protons of -OH in the theoretical studies may resonate in different regions. Calculated and experimental ^{1}H-NMR values of nucleosides **5a-c** are presented in **Table 2**.

The UV spectrum of nucleosides **5a-c** measured in five different solvents depending on polarities at various concentrations (10^6-10^8 M) between 300 and 700 nm. Nucleoside **5a** gave double maxima in all solvents. When the first maximums were compared, it is observed that the wavelengths did not change much. The most bathochromic shift at the wavelengths of the second maxima was in DMF. According to the λ_{max} in chloroform, hypochromic shift was observed in methanol. Nucleoside **5b** except for acetic acid, gave double maxima. Second maxima values of **5b** in DMF were shifted bathochromically, according to the λ_{max} of the others. Nucleoside **5c** gave single maxima in methanol, acetic acid, chloroform and double maxima in DMSO and DMF. Bathochromic shifts were the largest in DMSO and DMF when compared with others. Absorption spectrums of nucleosides **5a-c** were shown in **Fig. 6**.

Electronic transition wavelengths of the nucleosides **5a-c** were calculated for all solvents using the TD-DFT method with B3LYP/6-311G (d,p) level. Calculated and experimentally obtained λ_{max} (nm) values were listed in **Table 3**. The calculated λ_{max} values of nucleoside **5a-c** gave three maxima in all solvents and no significant change was observed. Excitation energies, oscillator strengths and absorbance of the nucleosides were also calculated in the DMF solvent using the TD-DFT method with same level of theory (**Table 4-6**). In electronic transitions of nucleosides **5b** and **5c**, the major contributions for each transition were calculated to occur only between one orbital couple. In the **5a** nucleosides, three or two orbital couples contributed to each electronic transition. The highest occupied molecular orbital (HOMO) and lowest unoccupied molecular orbital (LUMO) are known as boundary molecular orbitals and are the most important orbitals in molecular systems. Four important frontier molecular orbitals (HOMO-1, HOMO, LUMO and LUMO+1) were selected for each nucleosides and given in **Figure 7-9**. As can be seen from the diagrams, the frontier molecular orbitals were usually located over the benzene and pyrazole rings of the nucleosides **5a-c**. On

the other hand, it was determined that the ribofuranose skeletons did not fully contribute to HOMO and LUMO. The calculated HOMO energies for the nucleosides **5a**, **5b** and **5c** were -5.913, -6.077 and -6.178 eV, respectively while the LUMO energies were -2.173, -2.206 and -2.641 eV, respectively. The energy gap between HOMO and LUMO characterizes the molecular chemical stability [30]. The HOMO-LUMO energy ranges of the synthesized nucleosides were calculated to be 3.744, 3.871 and 3.537 eV, respectively. Moving from these values, it was thought that **5b** was the hardest and stable molecule among synthesized nucleosides. It is also expected that the nucleoside **5c** with the least HOMO-LUMO energy gap will be more reactive in chemical reactions.

3.2. Molecular structure

Geometry optimization of the synthesized nucleosides **5a-c** were done using B3LYP functional with 6-311G(d,p) basis set in gas phase. The fully optimized geometries of the **5a**, **5b** and **5c** including numbering atoms are shown in **Figure 10**, **11** and **12**, respectively. The values of the calculated bond lengths (Å), bond angles (^{o}) and dihedral angles (^{o}) are given in **Table 7**. In all three nucleosides, the shortest bond length was observed between the N12 and N13 atoms forming the azo group. The C-N bond between the benzene and the nitro group in the **5c** molecule was somewhat shorter than the other nucleosides. The calculated single bond length of C10-N12 for **5a**, **5b** and **5c** was found as 1.412, 1.419 and 1.417 Å, respectively which indicated that the shortest benzene-azo bond was located in molecule **5a**. As can be seen from **Table 4**, the bond lengths between atoms in pyrazole and ribofuranose structures were approximately the same for all three nucleosides. When the bond angles between the atoms in the nucleosides were examined, it was observed that the O-N-O bond angle in the nitro group of the compound **5a** was slightly larger, while the azo group was always connected to the benzene group at the same angle. The calculated value of the O26-N25-C11-

C10, O42-N41-C6-C11 and O42-N41-C7-C6 dihedral angle for the **5a**, **5b** and **5c** between benzene ring and oxygen atoms of nitro group was found as -142.2^{o}, -179.9^{o}, -179.9^{o}, respectively. This indicates that the benzene ring and the nitro group were not lying in the same plane in molecule **5a**. The same observation was observed between benzene and azo groups. The dihedral angle of C11-C10-N12-N13 was 35.7^{o} in the **5a** molecule, while it was calculated as -0.5^{o} and -0.2^{o} in **5b** and **5c**, respectively, indicating that the benzene ring and the azo group in the **5a** molecule were not lying in the same plane. Furthermore in the synthesized nucleosides the dihedral angles of C18-C19-C23-O24 were calculated to be around 170^{o}, indicating that the -CH_2OH group was present in the same plane with the ribofuranose ring in all three nucleosides.

3.3. Molecular electrostatic potential (MEP)

The surface emerging in the molecular electrostatic potential (MEP) diagram gives information on molecular size, shape, charge distribution and electrostatic potential value. These diagrams are important in determining the locations of the electrophilic and nucleophilic reactions in the molecule. In the MEP maps, the red parts represent the electronically rich regions of the molecule, while the blue parts represent the electronically poor regions. The molecular electrostatic potential (MEP) surfaces of the synthesized nucleosides **5a-c** were calculated using the B3LYP level of DFT using 6-311G(d,p) basis set, and the 3D maps are given in **Figure 13-15**.

When the MEP surfaces of the compounds were examined, it was seen that the regions with the highest electron density in the three molecules were around the oxygen atoms in the nitro group, which had a high electronegativity effect. Electron density was also observed on the oxygen atom in the ribofuranose ring. There is also some negative charge on the azo groups of

the molecules, while the azo group with the most electron-rich region is in the **5a** molecule. The blue regions in the molecules are on hydrogen atoms that are directly connected to the electronegative oxygen atoms. Thus, the regions with the lowest electron density in the synthesized nucleosides are around O-H groups attached to the pyrazole and ribofuranose rings.

3.4. Molecular docking studies

Investigation of protein and ligand interaction plays an important role in the design of structurally based drugs. In order to examine the antiproliferative activities of synthesized nucleoside analogues **5a-c**, a detailed intermolecular interaction between the ligands and biological targets were analyzed through application of molecular docking studies on the crystal structure of epidermal growth factor receptor (PDB ID: 1M17) and vascular endothelial growth factor receptor 2 (PDB ID: 2XIR). Binding energy, full fitness score and hydrogen bond location with length were found and results were given in **Table 8** and **9**.

These results showed that binding energy range of all compounds was between -6.35 and -10.35 kcal/mol and number of hydrogen bonds range was 2-5. The docking results showed that synthesized compounds fit well in the binding cavity of EGFR (**Figure 16, 17**) and VEGFR2. When binding energies were examined, it was determined that the interaction of all three ligands synthesized with EGFR was stronger than VEGFR2. The strongest interaction between (**5a-c**)- EGFR was in the **5b**- EGFR pair which has lowest interaction energy of -10.35 kcal/mol. This most stable docked pose showed five hydrogen bonding interactions with Leu 838, Glu 673, Glu 673, Ala 674, Ser 744 in the active site of EGFR.

The amino acid Glu 673 had formed two hydrogen bonding using OE2 and OE1 atoms with 2.746 and 1.713 Å bond lengths, respectively. Another hydrogen bond was observed at a

distance of 2.159 Å with Leu 838 and H atom of CH-OH moiety. Finally the amino acids Ala 674 (2.409 Å) and Ser 744 (2.901 Å) had formed hydrogen bonding with oxygen atoms of CH-OH and nitro groups, respectively. Full fitness scores of the studied molecules were found to be between 1671.46 and 2284.53. The good inhibition activity of **5b** compared to **5a** and **5c** was further confirmed by full fitness score. The calculated full fitness score for interaction **5b**-EGFR is 2284.53. The designed and synthesized compounds **5a-c** showed good activity and this was confirmed by the mode of orientation of these molecules with targets. Among the compounds **5a-c**, **5b** was considered as the best compound into the binding site of EGFR with the five hydrogen bonding, lowest binding energy (-10.35 kcal/mol) and highest full fitness score 2284.53.

4. Conclusion

Modified nucleosides have attracted interest in recent years because the showing interesting biological properties [31-33]. So, the design and synthesis of a three novel ribofuranose nucleosides **5a-c** were demonstrated in this report. Compounds were characterized by ^{1}H-NMR, FT-IR and UV-Vis spectroscopy. The molecular structural parameters, vibrational frequencies and chemical shifts of the fundamental modes, MEP, HOMO-LUMO analysis of the synthesized molecules were determined from DFT method utilizing 6-311G(d,p) basis set. It was found that theoretical spectroscopic results were in a good agreement with those of the experiments. Furthermore, the molecular docking simulations were performed using epidermal growth factor receptor (EGFR) and vascular endothelial growth factor receptor 2 (VEGFR2) to predict antiproliferative activity of the synthesized nucleosides. All three compounds studied inhibited both EGFR and VEGFR2, while the best interaction was observed between **5b**-EGFR with 5 hydrogen bonds and -10.35 kcal/mol binding energy. Based on the results of the molecular docking studies, nucleoside **5b** was found to have a very

high potential to inhibit the EGFR. These results can be very useful in the development of potential anticancer drugs.

References

[1] C. Simons, Carbocyclic Nucleosides. Gordon & Breach Science Publisher: Reading, UK, 2001, 137-153.

[2] L. Jordheim, C.M. Galmarini, and C. Dumontet, Nucleoside analogues and nucleobases in cancer treatment. Lancet. Oncol. 3 (2002) 415- 424.

[3] L. Jordheim, C.M. Galmarini, and C. Dumontet, Drug resistance to cytotoxic nucleoside analogues. Curr. Drug Targets. 4 (2003) 443-460.

[4] L. Jordheim, C.M. Galmarini, and C. Dumontet, Recent developments to improve the efficacy of cytotoxic nucleoside analogues. Anticancer Drug Discov. 1 (2006) 163-170.

[5] I.D. Kuntz, J.M. Blaney, S.J. Oatley, R. Langridge, and T.E. Ferrin, A geometric approach to macromolecule-ligand interactions. J. Mol. Biol. 161 (1982) 269-288.

[6] B.J. McConkey, V. Sobolev, and M. Edelman, The performance of current methods in ligand-protein docking. Curr. Sci. 83 (2002) 845-855.

[7] F. Ciardiello, and G. Tortora, Antiepidermal growth factor receptor drugs in cancer therapy. Expert. Opin. Investig. Drugs. 1 (2002) 755-768.

[8] P.M. Harari, Epidermal growth factor receptor inhibition startegies in oncology. Endocr. Relat. Cancer. 1 (2004) 689-708.

[9] A. Morabito, E. De Maio, M. Di Maio, N. Normanno, and F. Perronea, Tyrosine Kinase Inhibitors of Vascular Endothelial Growth Factor Receptors in Clinical Trials: Current Status and Future Directions. The Oncologist. 11 (2006) 753–764.

[10] M. Miettinen, M. Rikala, J. Rysz, J. Lasota, and Z. Wang, Vascular Endothelial Growth Factor Receptor 2 (Vegfr2) as a Marker for Malignant Vascular Tumors and Mesothelioma - Immunohistochemical Study of 262 Vascular Endothelial and 1640 Nonvascular Tumors. Am. J. Surg. Pathol. 36 (2012) 629–639.

[11] F. Cortés, C. Debacker, B. Peault, and M.C. Labastie, Differential expression of KDR/VEGFR-2 and CD34 during mesoderm development of the early human embryo. Mech. Dev. 83 (1999) 161-164.

[12] N.R Smith, D. Baker, N.H. James, K. Ratcliffe, M. Jenkins, S.E. Ashton, G. Sproat, R. Swann, N. Gray, A. Ryan, J.M. Jürgensmeier, and C. Womack, Vascular endothelial growth factor receptors VEGFR-2 and VEGFR-3 are localized primarily to the vasculature in human primary solid cancers. Clin. Cancer Res. 16 (2010) 3548–3561.

[13] C.R. Antonescu, A. Yoshida, T. Guo, N.E. Chang, L. Zhang, N.P. Agaram, L.X. Qin, M.F. Brennan, S. Singer, and R.G. Maki, KDR activating mutations in human angiosarcomas are sensitive to specific kinase inhibitors. Cancer Res. 69 (2009) 7175-7179.

[14] I.K. Dev, R.E. Dornsife, T.M. Hopper, J.A. Onori, C.G. Miller, L.E. Harrington, K.M. Dold, R.J. Mullin, J.H. Johnson, R.M. Crosby, A.T. Truesdale, A.H. Epperly, K.W. Hinkle, M. Cheung, J.A. Stafford, D.K. Luttrell, and R. Kumar, Antitumour efficacy of VEGFR2 tyrosine kinase inhibitor correlates with expression of VEGF and its receptor VEGFR2 in tumour models. Brit. J. Cancer. 91 (2004) 1391-1398.

[15] G. Korpanty, L.A. Sullivan, E. Smyth, D.N. Carney, and R.A. Brekken, Molecular and clinical aspects of targeting the VEGF pathway in tumors. J. Oncol. 2010 (2010) 652320-652332.

[16] F.M. Yakes, J. Chen, J. Tan, K. Yamaguchi, Y. Shi, P. Yu, F. Qian, F. Chu, F. Bentzien, B. Cancilla, J. Orf, A. You, A.D. Laird, S. Engst, L. Lee, J. Lesch, Y.C. Chou, and A.H. Joly, Cabozantinib (XL184), a novel MET and VEGFR2 inhibitor, simultaneously suppresses metastasis, angiogenesis, and tumor growth. Mol. cancer ther. 10 (2011) 2298-2308.

[17] J.C. Harmange, M.M. Weiss, J. Germain, A.J. Polverino, G. Borg, J. Bready, D. Chen, D. Choquette, A. Coxon, T. DeMelfi, L. DiPietro, N. Doerr, J. Estrada, J. Flynn, R.F. Graceffa, S.P. Harriman, S. Kaufman, D.S. La, A. Long, M.W. Martin, S. Neervannan, V.F.

Patel, M. Potashman, K. Regal, P.M. Roveto, M.L. Schrag, C. Starnes, A. Tasker, Y. Teffera, L. Wang, R.D. White, D.A. Whittington, and R. Zanon, Naphthamides as novel and potent vascular endothelial growth factor receptor tyrosine kinase inhibitors: design, synthesis, and evaluation. Med. Chem. 51 (2008) 1649-1667.

[18] K.J. Kim, B. Li, J. Winer, M. Armanini, N. Gillett, H.S. Phillips, and N. Ferrara, Inhibition of vascular endothelial growth factor-induced angiogenesis suppresses tumour growth in vivo. Nature. 362 (1993) 841-844.

[19] Gaussian 09, Revision E.01, M. J. Frisch, G. W. Trucks, H. B. Schlegel, G. E. Scuseria, M. A. Robb, J. R. Cheeseman, G. Scalmani, V. Barone, G. A. Petersson, H. Nakatsuji, X. Li, M. Caricato, A. Marenich, J. Bloino, B. G. Janesko, R. Gomperts, B. Mennucci, H. P. Hratchian, J. V. Ortiz, A. F. Izmaylov, J. L. Sonnenberg, D. Williams-Young, F. Ding, F. Lipparini, F. Egidi, J. Goings, B. Peng, A. Petrone, T. Henderson, D. Ranasinghe, V. G. Zakrzewski, J. Gao, N. Rega, G. Zheng, W. Liang, M. Hada, M. Ehara, K. Toyota, R. Fukuda, J. Hasegawa, M. Ishida, T. Nakajima, Y. Honda, O. Kitao, H. Nakai, T. Vreven, K. Throssell, J. A. Montgomery, Jr., J. E. Peralta, F. Ogliaro, M. Bearpark, J. J. Heyd, E. Brothers, K. N. Kudin, V. N. Staroverov, T. Keith, R. Kobayashi, J. Normand, K. Raghavachari, A. Rendell, J. C. Burant, S. S. Iyengar, J. Tomasi, M. Cossi, J. M. Millam, M. Klene, C. Adamo, R. Cammi, J. W. Ochterski, R. L. Martin, K. Morokuma, O. Farkas, J. B. Foresman, and D. J. Fox, Gaussian, Inc., Wallingford CT, 2016.

[20] GaussView, Revision 5.0.9, R. Dennington, T.A. Keith, and J.M. Millam, Semichem. Inc., Shawnee Mission, KS, 2009.

[21] A.D. Becke, Density-functional exchange-energy approximation with correct asymptotic behavior. Phys. Rev. A. 38 (1988) 3098-3100.

[22] C. Lee, W. Yang, and R.G. Parr, Development of the Colle-Salvetti correlation-energy formula into a functional of the electron density. Phys. Rev. B. 37 (1988) 785-789.

[23] R. Bauernschmitt, and R. Ahlrichs, Treatment of electronic excitations within the adiabatic approximation of time dependent density functional theory. Chem. Phys. Lett. 256 (1996) 454-464.

[24] M.E. Casida, C. Jamorski, K.C. Casida, and D.R. Salahub, Molecular excitation energies to high-lying bound states from time-dependent density-functional response theory: Characterization and correction of the time-dependent local density approximation ionization threshold. J. Chem. Phys. 108 (1998) 4439-4450.

[25] N.M. O'Boyle, A.L. Tenderholt, and K.M. Langner, cclib: A library for package-independent computational chemistry algorithms. J. Comp. Chem. 29 (2008) 839-845.

[26] R. Ditchfield, Molecular Orbital Theory of Magnetic Shielding and Magnetic Susceptibility. J. Chem. Phys. 56 (1972) 5688-5691.

[27] K. Wolinski, J.F. Hinton, and P. Pulay, Efficient implementation of the gauge-independent atomic orbital method for NMR chemical shift calculations. J. Am. Chem. Soc. 112 (1990) 8251-8260.

[28] A. Grosdidier, V. Zoete, and O. Michielin, SwissDock, a protein-small molecule docking web service based on EADock DSS. Nucleic Acids Res. 39 (2011) 270-277.

[29] E.F. Pettersen, T.D. Goddard, C.C. Huang, G.S. Couch, D.M. Greenblatt, E.C. Meng, and T.E. Ferrin, UCSF Chimera--a visualization system for exploratory research and analysis. J. Comput. Chem. 13 (2004) 1605-1612.

[30] K. Fukui, Role of frontier orbitals in chemical reactions. Science. 218 (1982) 747-754.

[31] L. Brulíková, P. Dzubák, M. Hajdúch, L. Lachnitová, M. Kollareddy, M. Kolár, K. Bogdanová, and J. Hlavác, Synthesis of 5-[alkoxy-(4-nitro-phenyl)-methyl]-uridines and study of their cytotoxic activity. Europ. J. Med. Chem. 45 (2010) 3588-3594.

[32] F. Seelaa, and X. Ming, 7-Functionalized 7-deazapurine b-D and b-L-ribonucleosides related to tubercidin and 7-deazainosine: glycosylation of pyrrolo[2,3-d]pyrimidines with 1-O-acetyl2,3,5-tri-O-benzoyl-b-D or b-L-ribofuranose. Tetrahedron. 63 (2007) 9850-9861.

[33] K. Taniho, R. Nakashima, M. Kandeel, Y. Kitamura, and Y. Kitade, Synthesis and biological properties of chemically modified siRNAs bearing 1-deoxy-D-ribofuranose in their 30 -overhang region. Bioorg. Med. Chem. Lett. 22 (2012) 2518-2521.

Figure Captions

Figure 1. The general route for the synthesis of nucleosides **5a-c.**

Figure 2. Tautomeric forms of the **5a-c** nucleosides**.**

Figure 3. Experimentally (upper) and theoretically (lower) FT-IR spectra of the **5a** nucleoside**.**

Figure 4. The linear regression between the experimental and theoretical frequencies of the **5a** (uppermost), **5b** (middle) and **5c** (undermost) nucleosides**.**

Figure 5. ^{1}H-NMR spectrum of the **5a** nucleoside.

Figure 6. The experimentally absorption spectrum of **5a** nucleoside.

Figure 7. Frontier molecular orbitals with energy values of the **5a** nucleoside calculated at B3LYP/6-311G(d,p) level

Figure 8. Frontier molecular orbitals with energy values of the **5b** nucleoside calculated at B3LYP/6-311G(d,p) level

Figure 9. Frontier molecular orbitals with energy values of the **5c** nucleoside calculated at B3LYP/6-311G(d,p) level

Figure 10. Optimized geometric structure of the **5a** nucleoside performed by B3LYP/6-311G(d,p) level

Figure 11. Optimized geometric structure of the **5b** nucleoside performed by B3LYP/6-311G(d,p) level

Figure 12. Optimized geometric structure of the **5c** nucleoside performed by B3LYP/6-311G(d,p) level

Figure 13. Molecular electrostatic potential map of the **5a** nucleoside calculated at B3LYP/6-311G(d,p) level.

Figure 14. Molecular electrostatic potential map of the **5b** nucleoside calculated at B3LYP/6-311G(d,p) level.

Figure 15. Molecular electrostatic potential map of the **5c** nucleoside calculated at B3LYP/6-311G(d,p) level.

Figure 16. Interacting mode of the **5b** nucleoside with EGFR (PDB ID: 1M17)

Figure 17. The binding of the **5b** nucleoside in the cavity of EGFR (PDB ID: 1M17)

Figure 1.

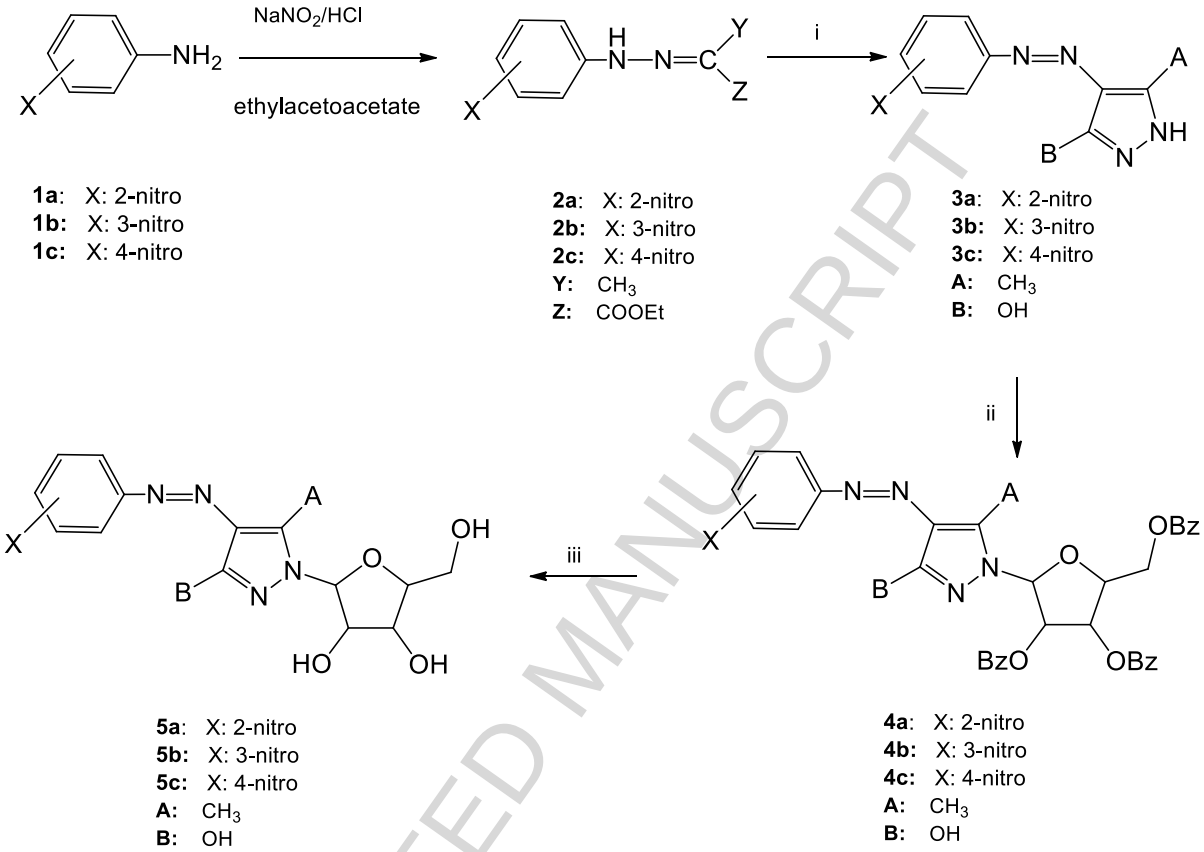

1a: X: 2-nitro
1b: X: 3-nitro
1c: X: 4-nitro

2a: X: 2-nitro
2b: X: 3-nitro
2c: X: 4-nitro
Y: CH_3
Z: COOEt

3a: X: 2-nitro
3b: X: 3-nitro
3c: X: 4-nitro
A: CH_3
B: OH

4a: X: 2-nitro
4b: X: 3-nitro
4c: X: 4-nitro
A: CH_3
B: OH

5a: X: 2-nitro
5b: X: 3-nitro
5c: X: 4-nitro
A: CH_3
B: OH

i) hydrazine hydrate
ii) hexamethyldisilazane, $(NH_4)_2SO_4$, 1-O-acetyl-2,3,5-tri-O-benzoyl-beta-D-ribofuranose, trimethylsilyl trifluoro-methanesulphonate, 1,2-dichloroethane
iii) MeOH/NH_3

Figure 2.

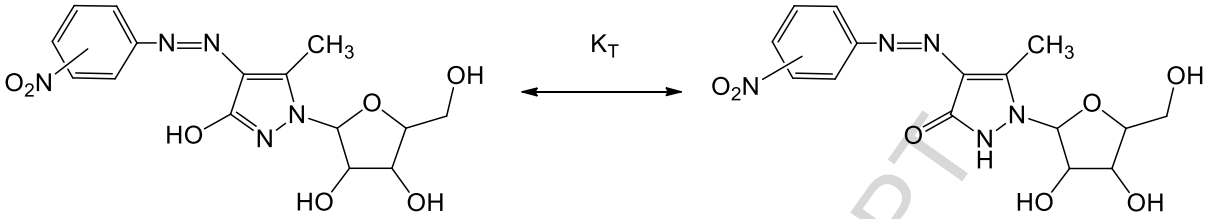

Figure 3.

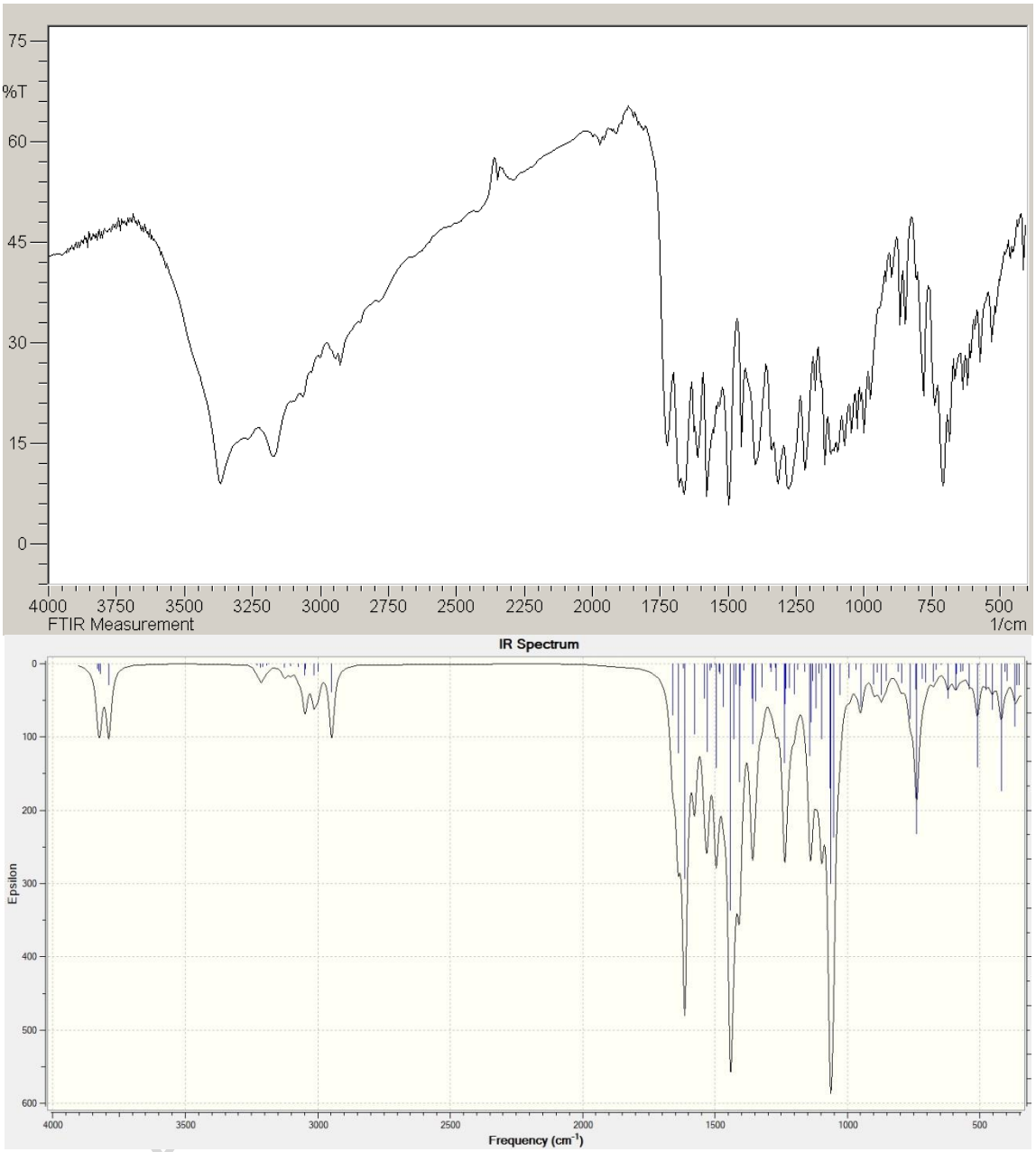

Figure 4.

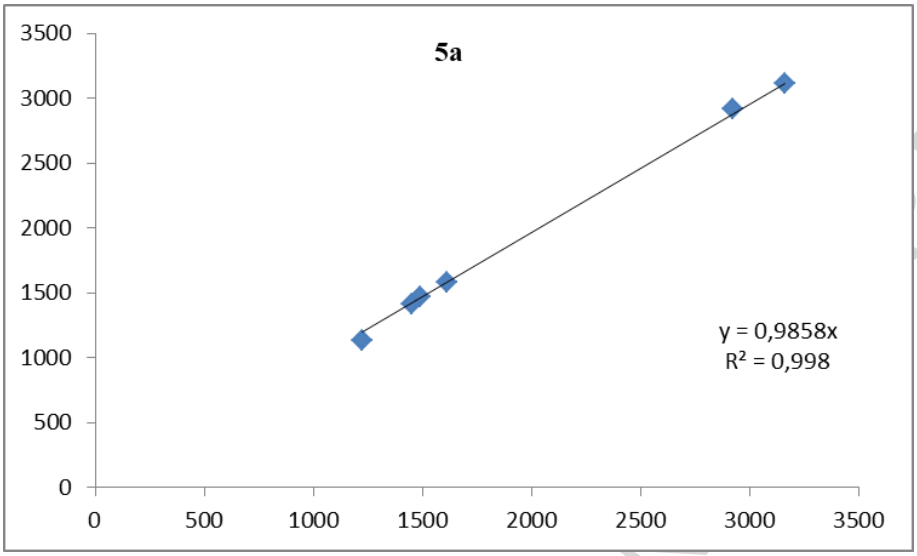

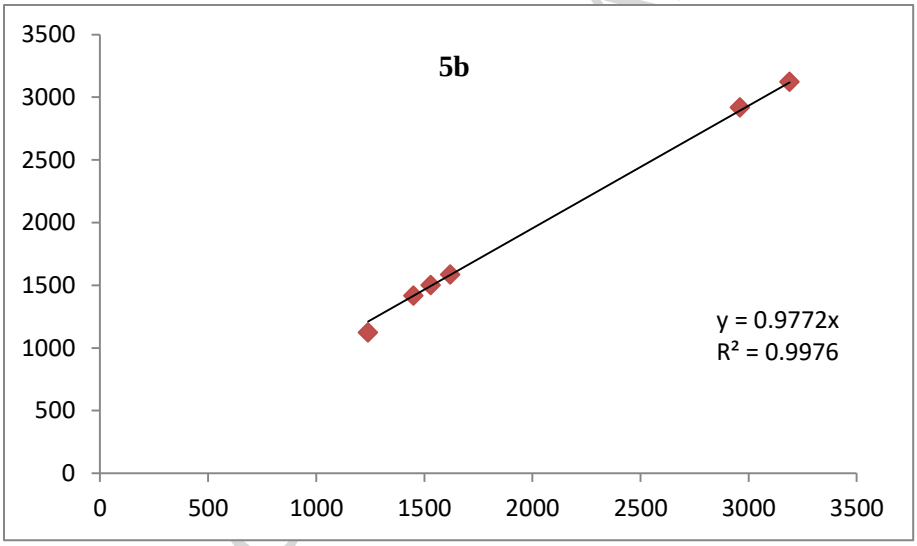

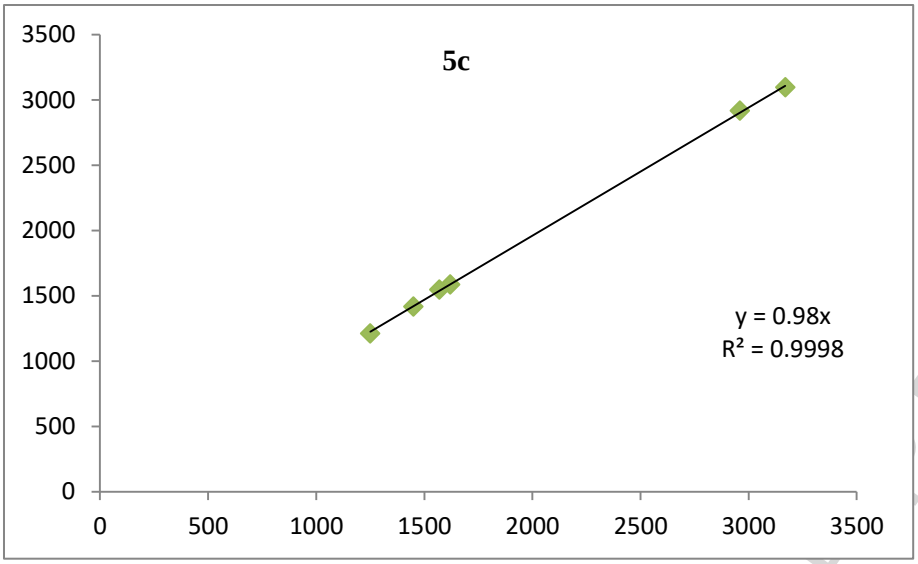

Figure 5.

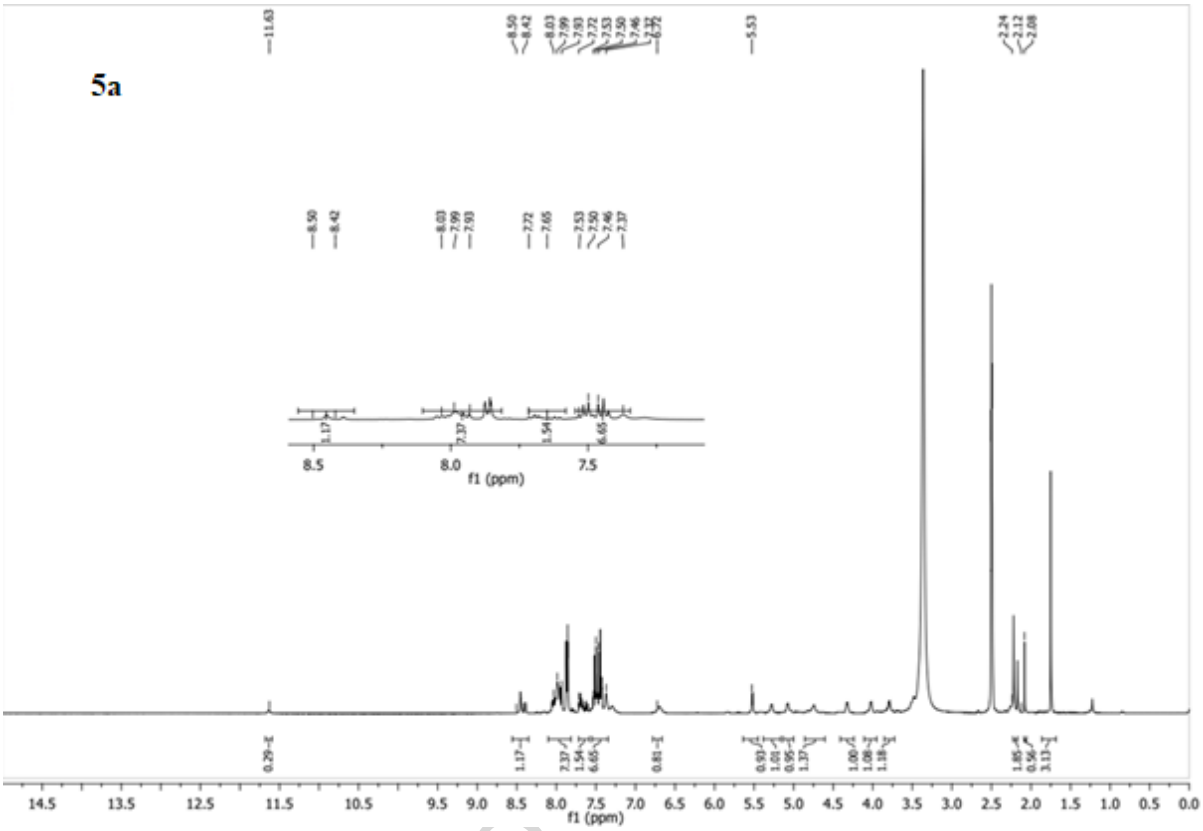

Figure 6.

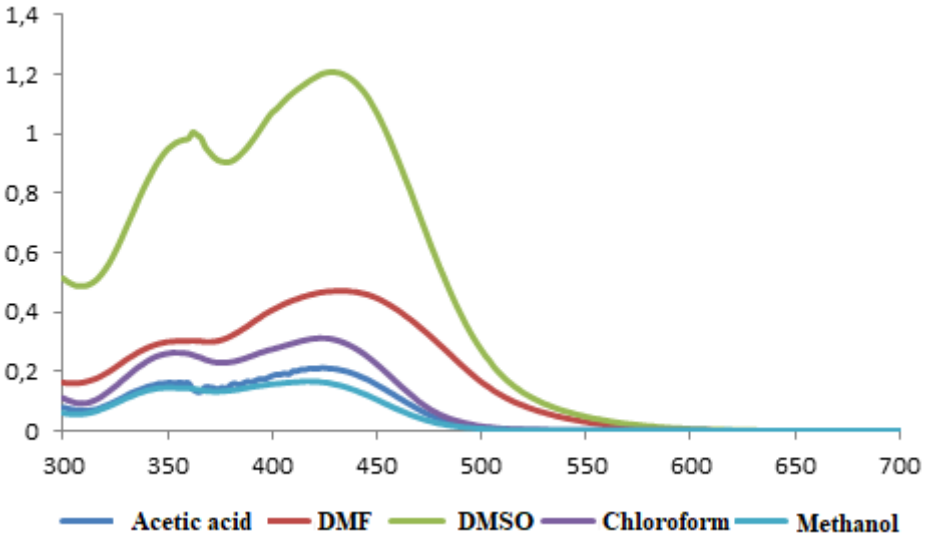

Figure 7.

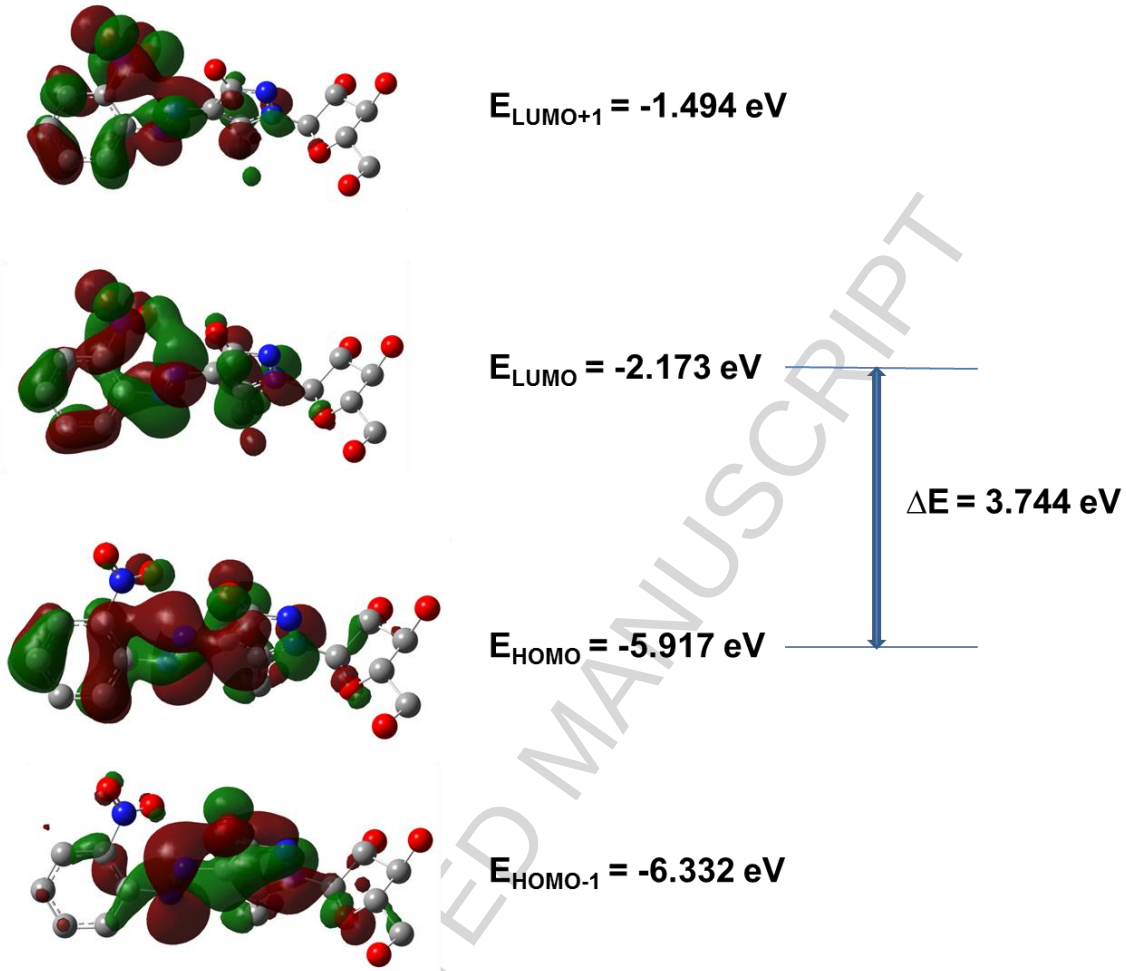

Figure 8.

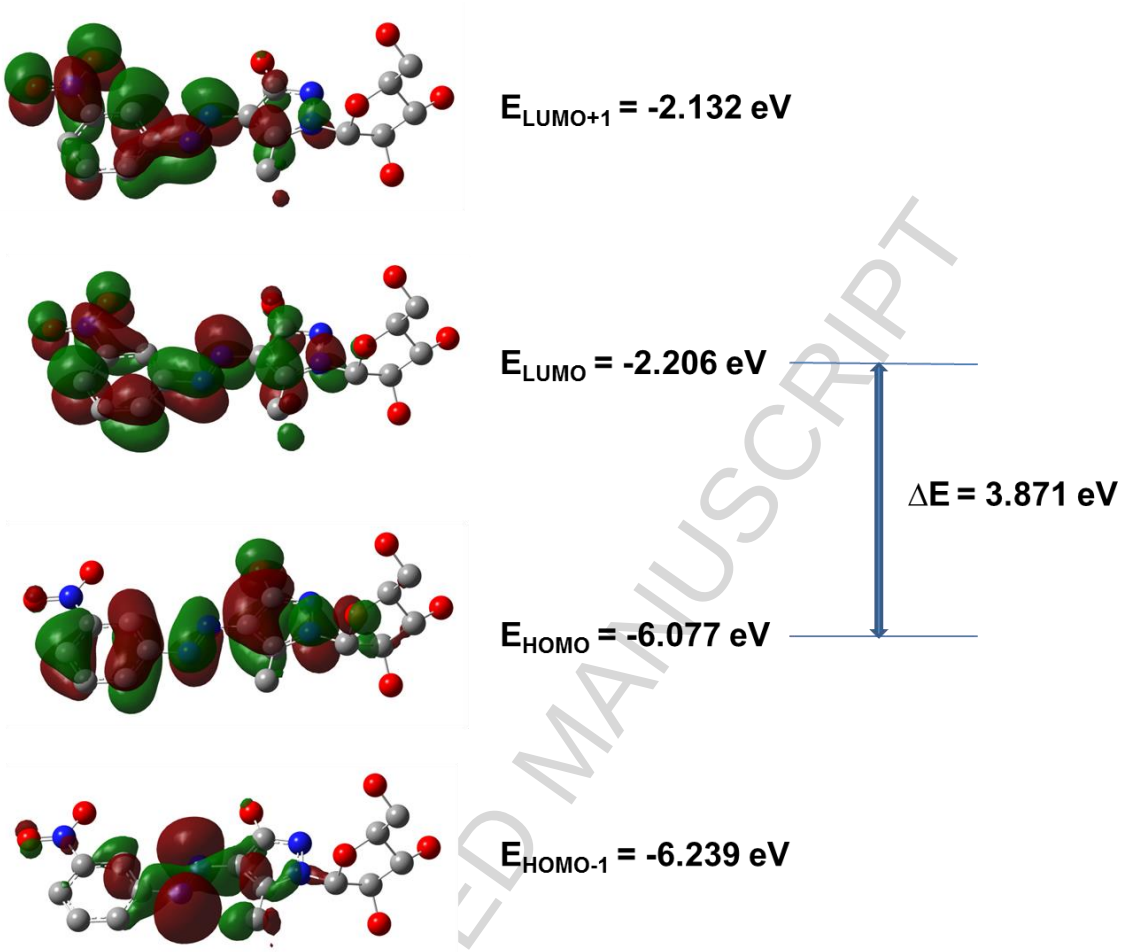

Figure 9.

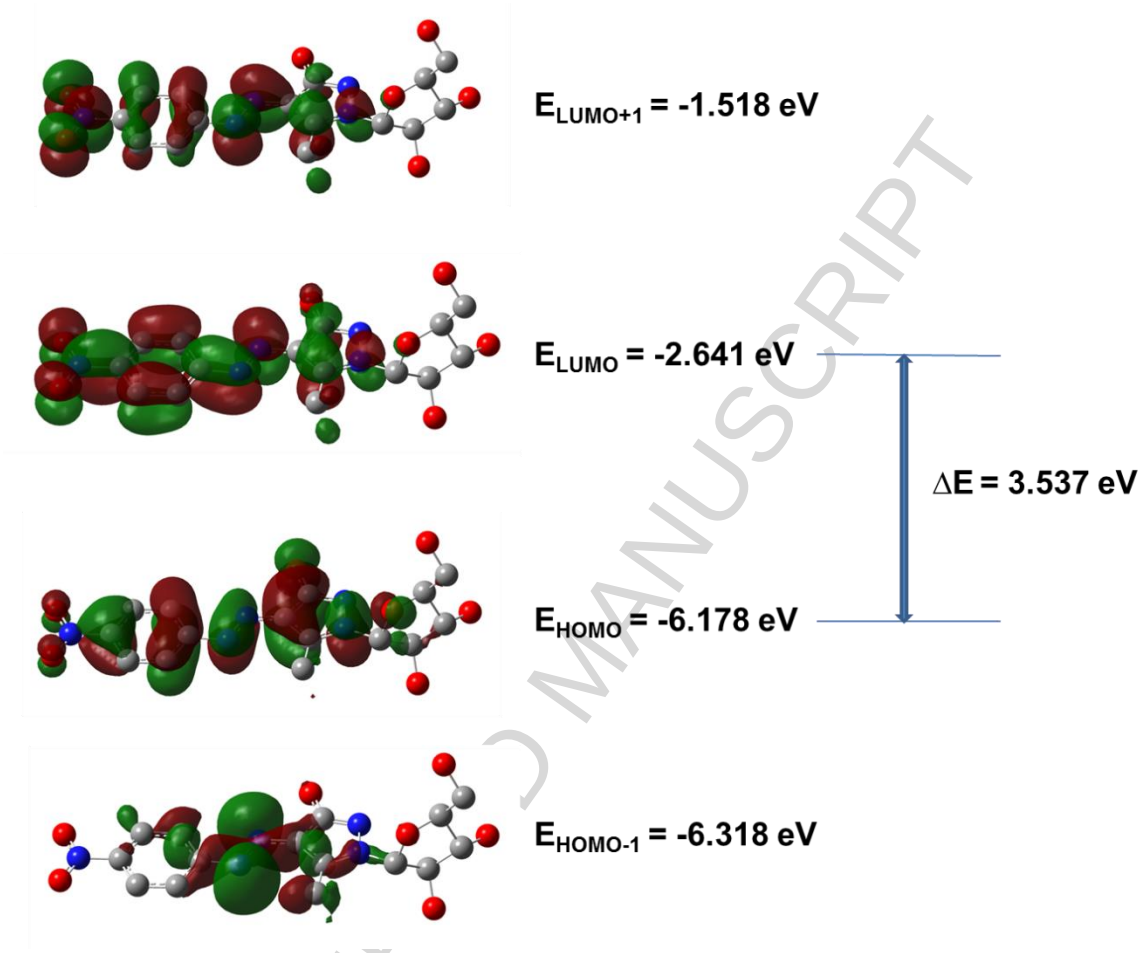

Figure 10.

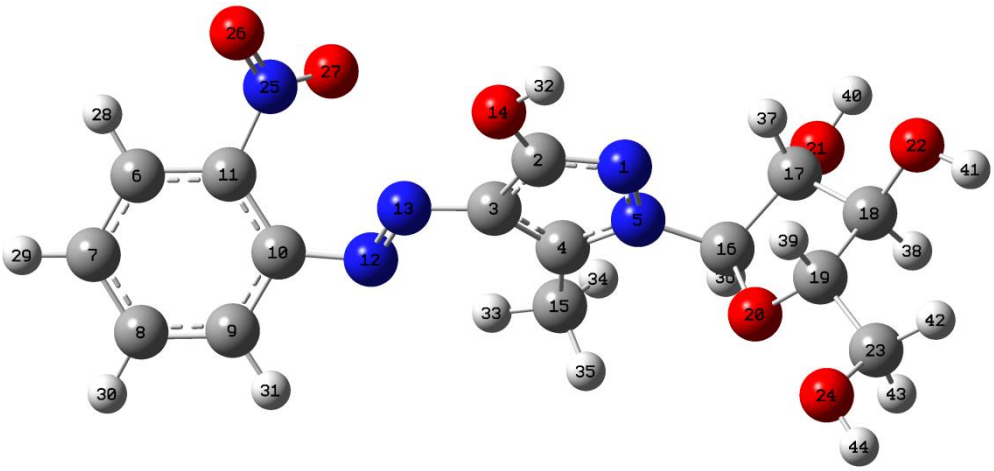

Figure 11.

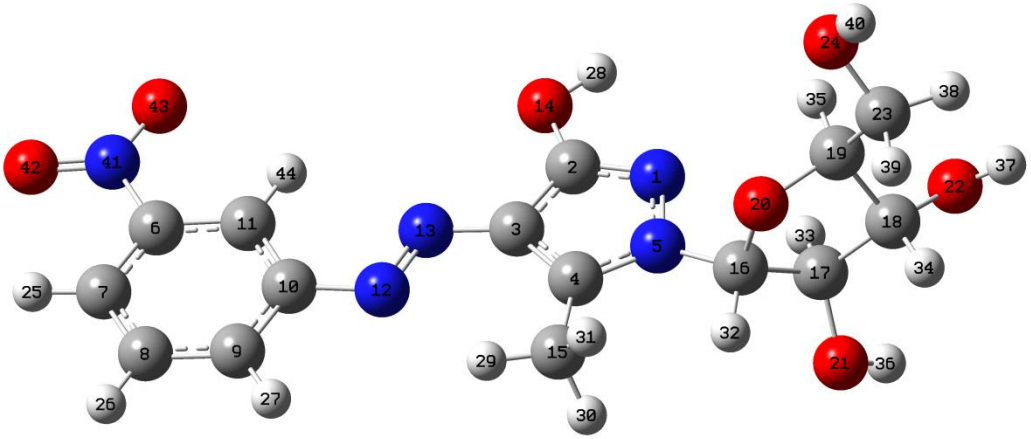

Figure 12.

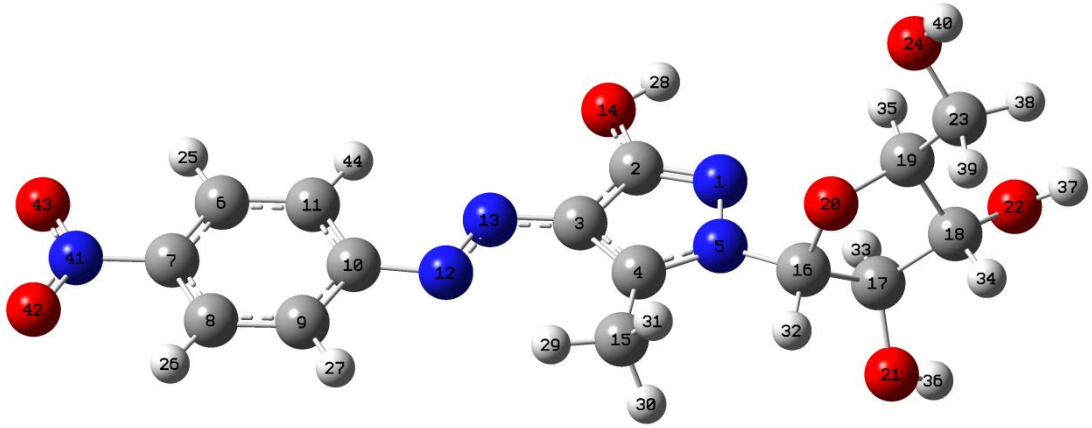

Figure 13.

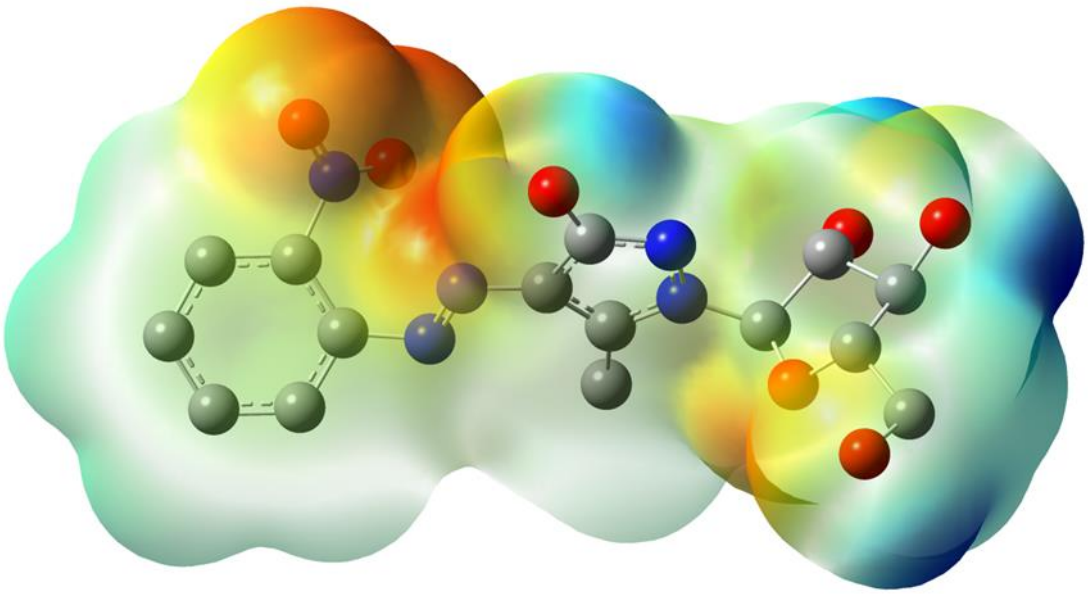

Figure 14.

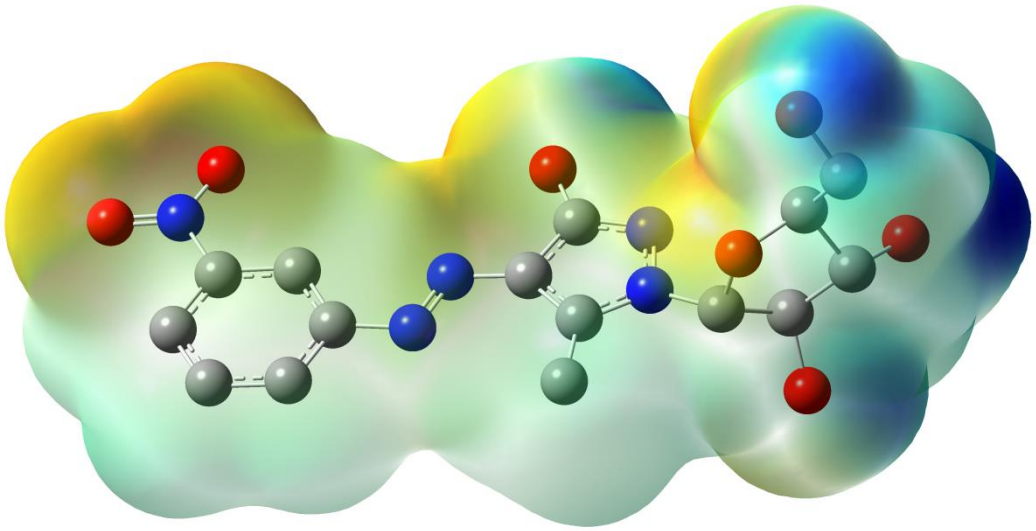

Figure 15.

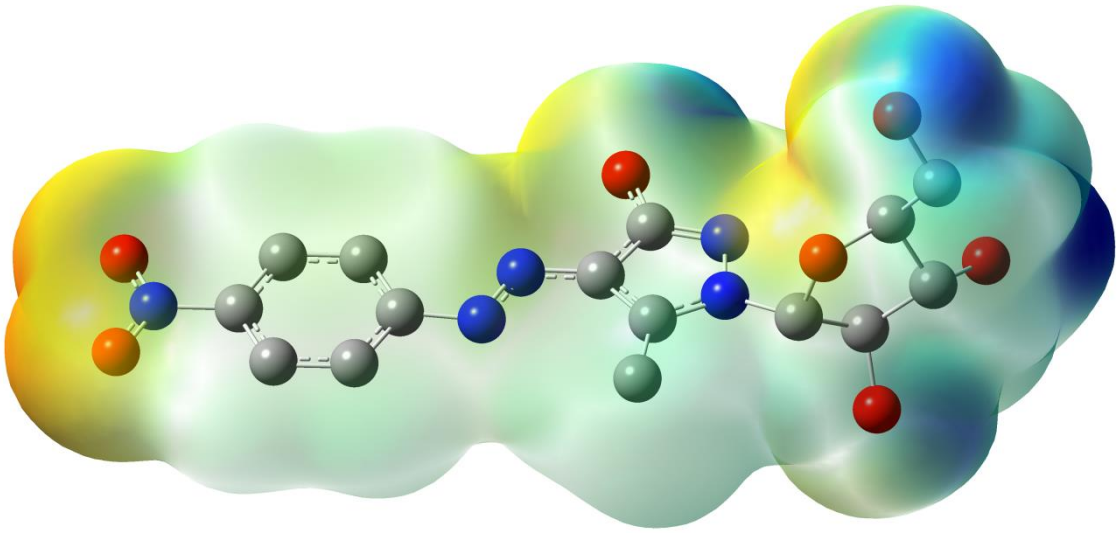

Figure 16.

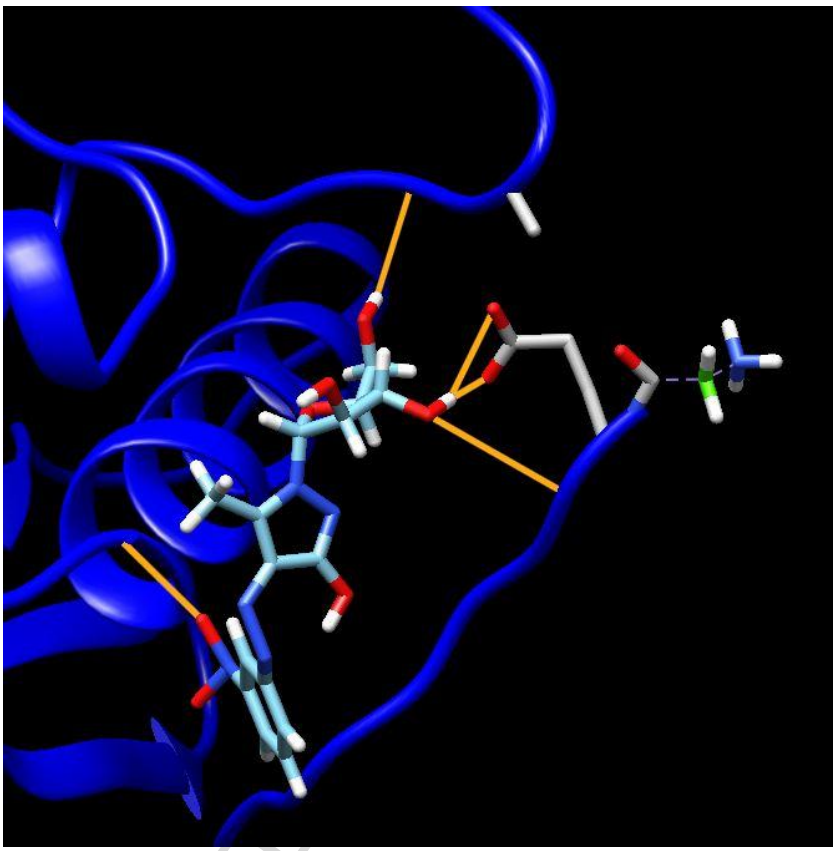

Figure 17.

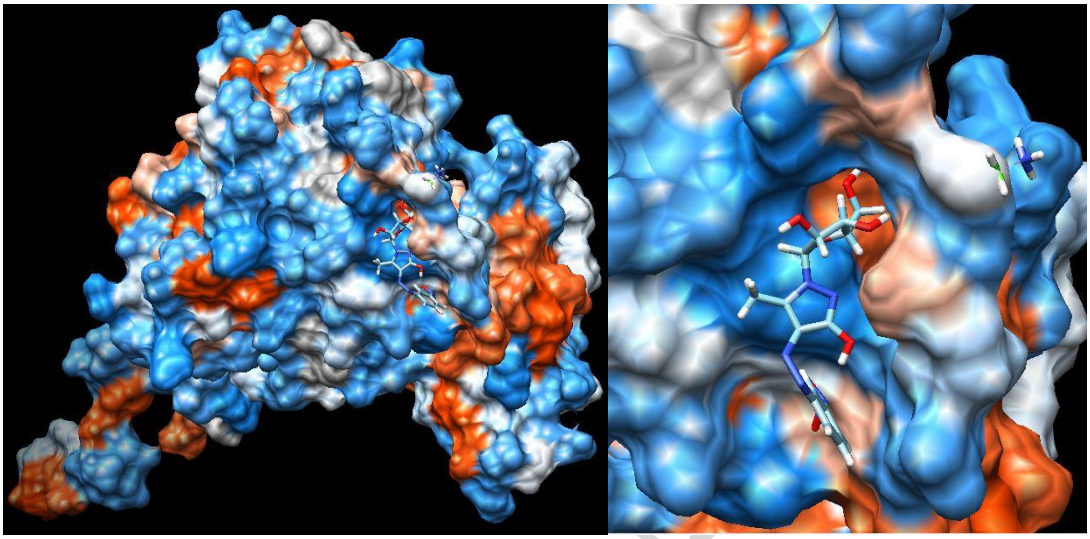

Table Captions

Table 1. FT-IR experimental values with those obtained from B3LYP/6-31G(d) method

Table 2. ^{1}H-NMR experimental values with those calculated from DFT method.

Table 3. The results of λmax (nm) obtained by experimentally and theoretically.

Table 4. The experimental, theoretical electronic transitions, excitation energies (eV), oscillator strengths (f) and major contributions of the **5a** nucleoside in DMF

Table 5. The experimental, theoretical electronic transitions, excitation energies (eV), oscillator strengths (f) and major contributions of the **5b** nucleoside in DMF

Table 6. The experimental, theoretical electronic transitions, excitation energies (eV), oscillator strengths (f) and major contributions of the **5c** nucleoside in DMF

Table 7. Some selected calculated bond lengths (Å), bond and dihedral angles (^{o}) for the **5a-c** nucleosides at the B3LYP/6-311G(d,p) level

Table 8. Binding energy, full fitness score hydrogen bond location with length within the (5a-c)-EGFR couples (PDB ID: 1M17)

Table 9. Binding energy, full fitness score hydrogen bond location with length within the (5a-c)-VEGFR2 couples (PDB ID: 2XIR)

Table 1.

	Experimental						B3LYP/6-311G(d,p)					
	ν_{Ar-H}	ν_{Alip-H}	$\nu_{N=N}$	$\nu_{N-Oasym}$	ν_{N-Osym}	ν_{C-O}	ν_{Ar-H}	ν_{Alip-H}	$\nu_{N=N}$	$\nu_{N-Oasym}$	ν_{N-Osym}	ν_{C-O}
5a	3160	2920	1490	1610	1450	1220	3113	2918	1471	1585	1416	1129
5b	3190	2960	1530	1620	1450	1240	3122	2919	1502	1586	1417	1123
5c	3170	2960	1570	1620	1450	1250	3095	2918	1546	1586	1417	1211

Table 2.

	Experimental (DMSO)			B3LYP/6-311G(d,p)		
	Aro.-H	**Alip.-H**	**X-H**	**Aro.-H**	**Alip.-H**	**X-H**
5a	7.37 – 8.50 (m. 4H)	2.08 (pyrazole, CH_3) 5.09-5.29 (ribofuranose,-CH, 2H) 5.53 (ribofuranose, -CH_2, 1H)	3.79-4.30 (ribofuranose,OH, 3H) 11.63 (pyrazole, OH)	7.68 – 8.04 (m. 4H)	2.33 (pyrazole, CH_3) 4.02-5.68 (ribofuranose,-CH) 4.11 (ribofuranose, -CH_2)	0.63-1.67 (ribofuranose,OH) 5.44 (pyrazole, OH)
5b	7.45 – 8.46 (m. 4H)	2.50 (pyrazole, CH_3) 4.03-5.67 (ribofuranose,-CH) 4.12 (ribofuranose, -CH_2)	3.79-4.34 (ribofuranose,OH) 11.62 (pyrazole, OH)	8.01 – 8.97 (m. 4H)	2.32 (pyrazole, CH_3) 4.03-5.67 (ribofuranose,-CH) 4.12 (ribofuranose, -CH_2)	0.66-1.65 (ribofuranose,OH) 5.57 (pyrazole, OH)
5c	7.35 – 8.29 (m. 4H)	2.50 (pyrazole,CH_3) 5.08-5.28 (ribofuranose,-CH, 2H) 5.51 (ribofuranose, -CH_2, 1H)	3.81-4.71 (ribofuranose,OH, 4H) 11.52 (pyrazole, OH)	8.18 – 8.79 (m. 4H)	2.37 (pyrazole,CH_3) 4.02-5.69 (ribofuranose,-CH) 4.12 (ribofuranose, -CH_2)	0.65-1.65 (ribofuranose,OH) 5.59 (pyrazole, OH)

Table 3.

	Experimental					B3LYP/6-311G(d,p)				
	DMSO	**DMF**	**Methanol**	**Acetic Acid**	**Chloroform**	**DMSO**	**DMF**	**Methanol**	**Acetic Acid**	**Chloroform**
5a	428-362	432-362	418-352	424-356	426-356	461-382-356	462-382-355	461-381-355	462-378-353	463-377-353
5b	408-352	424-344	366-350	382	386-366	457-394-385	457-394-385	456-393-384	458-389-382	459-388-381
5c	540-414	540-366	400	412	404	500-405-367	500-405-367	500-403-366	500-401-364	499-402-363

Table 4.

Transitions	Experimental		Theoretical B3LYP/6-311G(d,p)			
	λ (nm)	**E (eV)**	**λ (nm)**	**E (eV)**	**f**	**Major contributions**
$\pi \rightarrow \pi^*$ (benzene)	362	3.43	355	3.49	0.0895	H→L+1 (38%) H-1→L (37%) H-1→L+1 (12%)
$\pi \rightarrow \pi^*$ (azo)	-	-	382	3.25	0.1829	H→L (38%) H-1→L (27%) H→L+1 (26%)
$n \rightarrow \pi^*$	432	2.87	462	2.68	0.0880	H→L (58%) H-1→L (23%)

Table 5.

Transitions	Experimental		Theoretical B3LYP/6-311G(d,p)			
	λ (nm)	E (eV)	λ (nm)	E (eV)	f	Major contributions
$\pi \rightarrow \pi^*$ (benzene)	344	3.60	385	3.22	0.0006	H-1→L (96%)
$\pi \rightarrow \pi^*$ (azo)	-	-	394	3.15	0.0137	H→L (94%)
$n \rightarrow \pi^*$	424	2.92	457	2.71	0.0006	H-1→L+1 (98%)

Table 6.

Transitions	Experimental		Theoretical B3LYP/6-311G(d,p)			
	λ (nm)	**E (eV)**	**λ (nm)**	**E (eV)**	**f**	**Major contributions**
$\pi \rightarrow \pi^*$ (benzene)	366	3.39	367	3.38	0.1229	H-2→L (96%)
$\pi \rightarrow \pi^*$ (azo)	-	-	405	3.06	0.9504	H→L (97%)
$n \rightarrow \pi^*$	540	2.30	500	2.48	0.0006	H-1→L (87%)

Table 7.

5a		5b		5c	
Parameters	**B3LYP/ 6-311G(d,p)**	**Parameters**	**B3LYP/ 6-311G(d,p)**	**Parameters**	**B3LYP/ 6-311G(d,p)**
Bond lengths (Å)					
C11-N25	1.473	C6-N41	1.476	C7-N41	1.467
C10-N12	1.412	C10-N12	1.419	C10-N12	1.417
N12-N13	1.268	N12-N13	1.268	N12-N13	1.270
C3-N13	1.377	C3-N13	1.378	C3-N13	1.376
C2-O14	1.341	C2-O14	1.342	C2-O14	1.342
C4-C15	1.494	C4-C15	1.495	C4-C15	1.495
N5-C16	1.455	N5-C16	1.455	N5-C16	1.456
C16-O20	1.420	C16-O20	1.421	C16-O20	1.420
C18-O22	1.417	C18-O22	1.417	C18-O22	1.417
C19-C23	1.514	C19-C23	1.514	C19-C23	1.514
C23-O24	1.416	C23-O24	1.416	C23-O24	1.416
Bond angles (^{o})					
O26-N25-027	125.2	O42-N41-O43	124.6	O42-N41-O43	124.4
C11-N25-O27	117.7	C6-N41-O43	117.8	C7-N41-O43	117.8
C10-N12-N13	113.2	C10-N12-N13	113.6	C10-N12-N13	113.6
C3-C2-O14	125.0	C3-C2-O14	124.9	C3-C2-O14	124.9

O14-C2-N1	122.6	O14-C2-N1	122.6	O14-C2-N1	122.5
N1-N5-C16	118.5	N1-N5-C16	118.7	N1-N5-C16	118.7
C15-C4-N5	123.6	C15-C4-N5	123.5	C15-C4-N5	123.5
C16-C17-O21	109.0	C16-C17-O21	109.1	C16-C17-O21	109.1
C19-C18-O22	115.8	C19-C18-O22	115.9	C19-C18-O22	115.8
C19-C23-O24	108.9	C19-C23-O24	108.9	C19-C23-O24	108.9
Dihedral angles (^{o})					
O26-N25-C11-C10	-142.2	O42-N41-C6-C11	-179.9	O42-N41-C7-C6	-179.9
C11-C10-N12-N13	35.7	C11-C10-N12-N13	-0.5	C11-C10-N12-N13	-0.2
N1-N5-C16-O20	73.4	N1-N5-C16-O20	74.1	N1-N5-C16-O20	74.1
O21-C17-C18-O22	87.8	O21-C17-C18-O22	86.8	O21-C17-C18-O22	86.9
O22-C18-C19-C23	-82.4	O22-C18-C19-C23	-82.5	O22-C18-C19-C23	-82.5
C18-C19-C23-O24	170.6	C18-C19-C23-O24	170.7	C18-C19-C23-O24	170.7

Table 8.

Ligand	ΔG (kcal/mol)	Full Fitness Score	H Bond Location (Length)
5a	-8.44	2262.79	O of CH-OH & N-H of Cys 773 (2.470 Å)
			O of N-O & N-H of Ala 698 (2.270 Å)
5b	-10.35	2284.53	H of CH-OH & O of Leu 838 (2.159 Å)
			H of CH-OH & OE2 of Glu 673 (2.746 Å)
			H of CH-OH & OE1 of Glu 673 (1.713 Å)
			O of CH-OH & N-H of Ala 674 (2.409 Å)
			O of N-O & N-H of Ser 744 (2.901 Å)
5c	-7.87	2282.30	H of CH-OH & OE1 of Glu 673 (2.032 Å)
			O of CH_2-OH & OE1 of Glu 673 (2.731 Å)
			N of C=N & N-H of Asn 676 (2.326 Å)
			O of C-OH & N-H of Asn 676 (2.279 Å)
			O of N-O & N-H of Ala 678 (3.317 Å)

Table 9.

Ligand	ΔG (kcal/mol)	Full Fitness Score	H Bond Location (Length)
5a	-6.35	1671.46	O of N-O & N-H of Asp 126 (2.418 Å)
			O of CH-OH & N-H of Asn 168 (2.379 Å)
			H of CH-OH & O of Ser 165 (2.685 Å)
5b	-7.92	1683.11	H of CH-OH & O of Asp 126 (2.090 Å)
			H of C=N & N-H of Lys 167 (2.443 Å)
			O of CH-OH & N-H of Lys 167 (2.044 Å)
5c	-8.08	1688.16	O of N-O & HT1 of Hse 1 (2.058 Å)
			O of N-O & N-H of Cys 2 (2.317 Å)
			O of N-O & N-H of Glu 3 (3.453 Å)
			O of N-O & N-H of Glu 3 (3.162 Å)

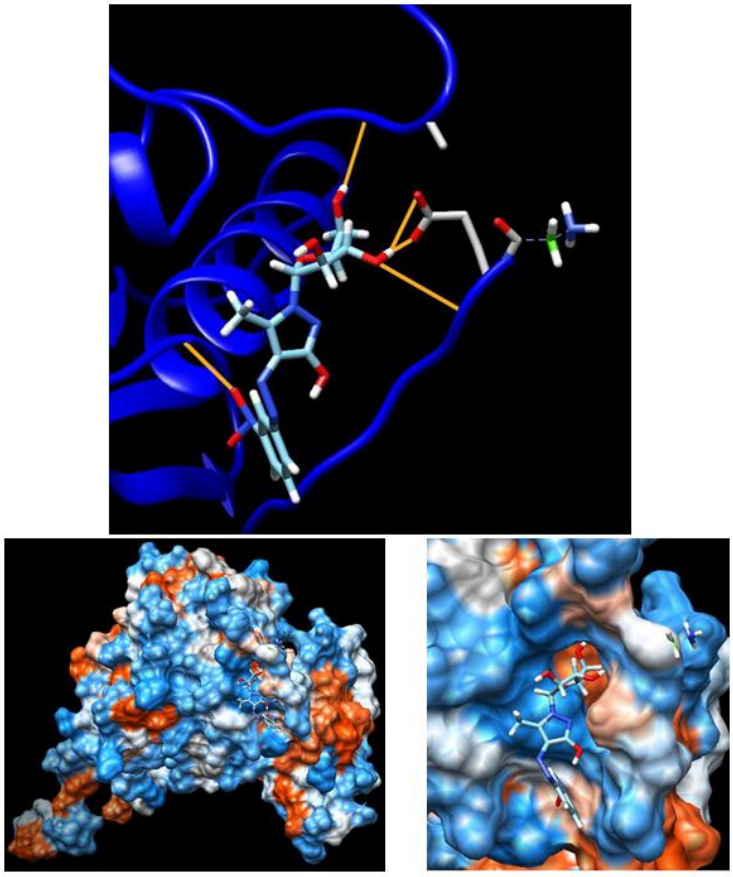

Graphical abstract

Highlights

- Three novel azo compounds containing ribofuranose moiety were synthesized
- Quantum chemical calculations were done by using B3LYP/6-311G(d,p) level of theory
- Experimental results were in agreement with those obtained from DFT calculations
- Molecular docking studies were performed using two different growth factor receptors
- *m*-nitro substitute azo molecule was found to have a potential to inhibit the EGFR